Supporting Information

Nitrogen-Doped $MoS_2/Ti_3C_2T_X$ Heterostructures as Ultra-Efficient Alkaline HER Electrocatalysts

Dong Liu[1,2,§], Zepeng Lv[1,2,§], Jie Dang[1,2,*], Wansen Ma[1,2], Kailiang Jian[1,2], Meng Wang[1,2], Dejun Huang[3], Weiqian Tian[4,*]

[1]College of Materials Science and Engineering, Chongqing University, Chongqing 400044, PR China

[2]Chongqing Key Laboratory of Vanadium-Titanium Metallurgy and New Materials, Chongqing University, Chongqing 400044, PR China

[3]Spectris Instrumentation and Systems Shanghai Ltd., Shanghai 200233, PR China

[4]Department of Fibre and Polymer Technology, KTH Royal Institute of Technology, Teknikringen 56, 10044 Stockholm, Sweden

***Corresponding author:**

Jie Dang

E-mail: jiedang@cqu.edu.cn

Phone: +86-23-65112631; Fax: +86-23-65112631

Address: College of Materials Science and Engineering, Chongqing University, Chongqing 400044, PR China

ORCID: https://orcid.org/0000-0003-1383-8390

Weiqian Tian

E-mail: weiqian@kth.se

Address: Department of Fibre and Polymer Technology, KTH Royal Institute of Technology, Teknikringen 56, 10044 Stockholm, Sweden

ORCID: https://orcid.org/0000-0003-3497-2054

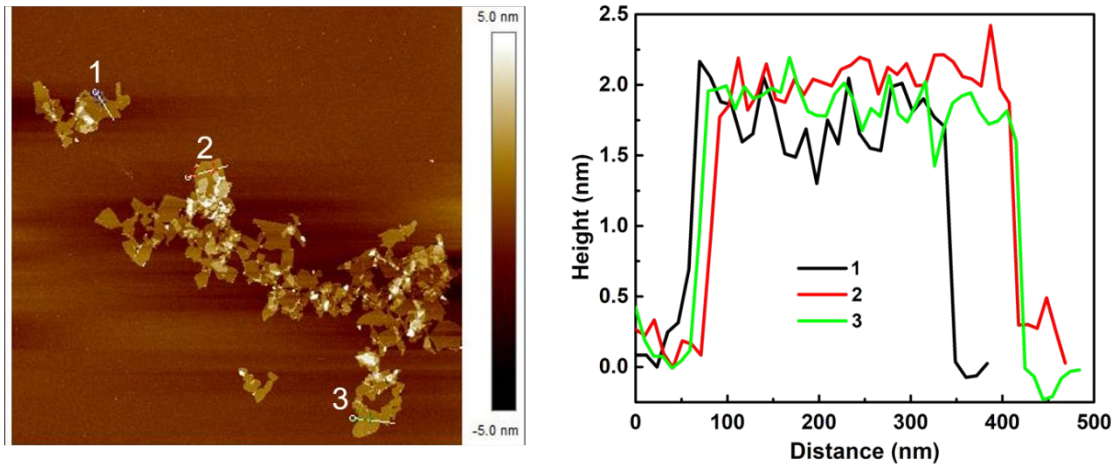

Figure S1. The AFM image and the corresponding height profile of single-layer $Ti_3C_2T_X$

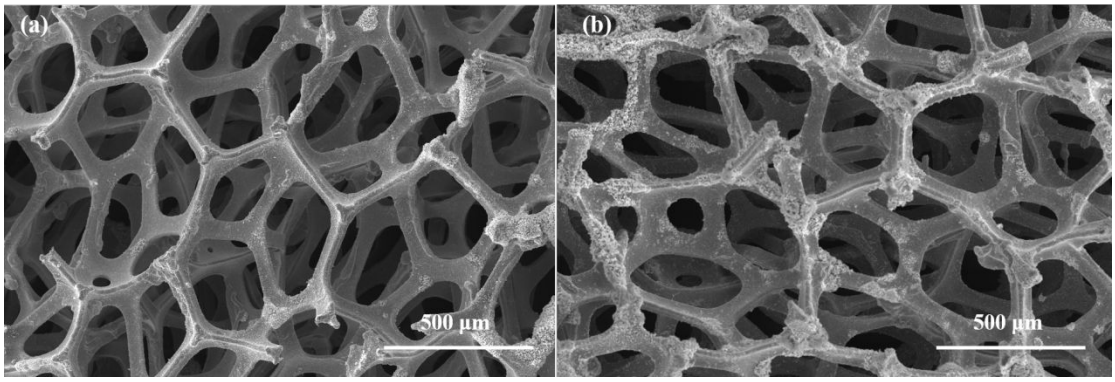

Figure S2. The SEM images of (a) $MoS_2/Ti_3C_2T_X$ and (b) N-doped $MoS_2/Ti_3C_2T_X$ heterostructures on Nickel foam.

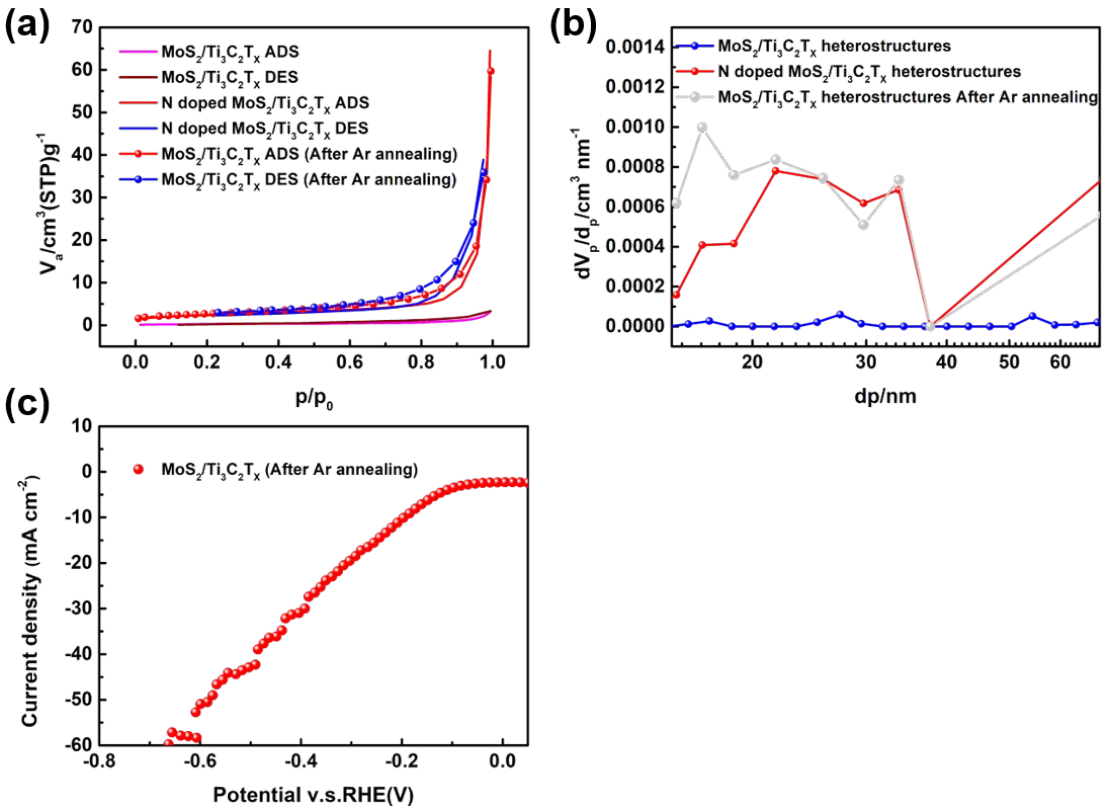

Figure S3. (a) N_2 adsorption-desorption isotherms and (b) the pore size distribution of N-doped $MoS_2/Ti_3C_2T_X$ heterostructures and $MoS_2/Ti_3C_2T_X$ heterostructures on Ni foam. (c) LSV curves of $MoS_2/Ti_3C_2T_X$ heterostructures after Ar annealing in 1.0 M KOH

Then we annealed $MoS_2/Ti_3C_2T_X$ heterostructures in Ar. We found that the pore size distributions of $MoS_2/Ti_3C_2T_X$ heterostructures and N-doped $MoS_2/Ti_3C_2T_X$ heterostructures are not much different, but the overpotential of N-doped $MoS_2/Ti_3C_2T_X$ heterostructures (80 mV at 10 mA cm^{-2}) is much smaller than that of $MoS_2/Ti_3C_2T_X$ heterostructures (195 mV at 10 mA cm^{-2}), thus indicating that the main source of activity in N-doped $MoS_2/Ti_3C_2T_X$ heterostructures is not microstructure difference but N-doped.

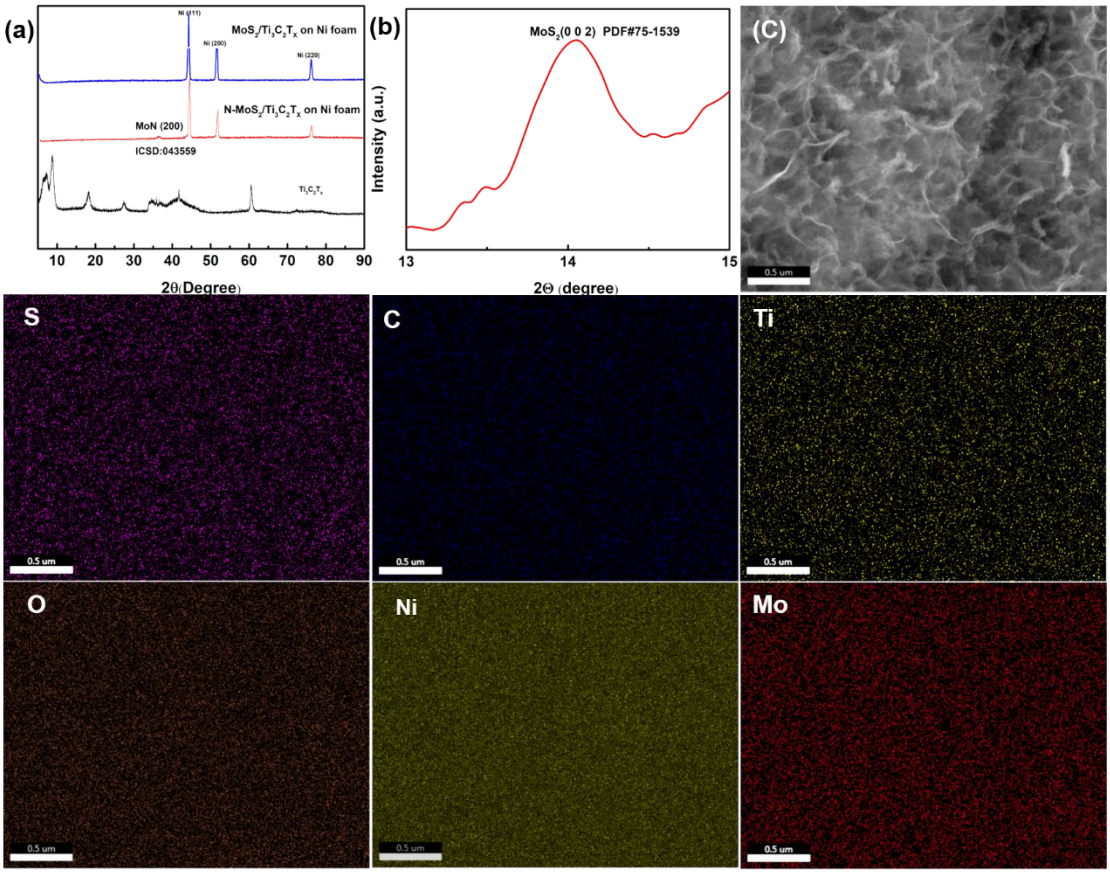

Figure S4 (a) The XRD patterns of $MoS_2/Ti_3C_2T_X$ Heterostructures on Ni foam, and N-doped $MoS_2/Ti_3C_2T_X$ Heterostructures on Ni foam. and (b) The low-angle XRD patterns of $MoS_2/Ti_3C_2T_X$ Heterostructures (c) $MoS_2/Ti_3C_2T_X$ heterostructures on Ni foam SEM and the corresponding EDS mapping images.

As shown in Figure S4a, the patterns of samples coating on Ni foam show obvious Ni peak (PDF#04-0850) and week diffraction peaks of MoS_2 that is due to low mass loading of $MoS_2/Ti_3C_2T_x$ compared to the crystal Ni foam as the frameworks. According to previous studies, the dried restacked $Ti_3C_2T_x$ nanosheets show obvious XRD diffraction, in line with our XRD pattern of the $Ti_3C_2T_x$ precursor (Figure S4a). However, no obvious diffraction can be observed in the final $MoS_2/Ti_3C_2T_x$ heterostructures on Ni foam. This result may be explained by the relatively low content of the $Ti_3C_2T_x$ in the hybrid, as well as the inhibition of the restacking of $Ti_3C_2T_x$ nanosheets by the MoS_2 crystallites. The low-angle XRD pattern of $MoS_2/Ti_3C_2T_X$ heterostructures (Figure S4b) shows the MoS_2 (002) plane. After

nitridation process, the MoS_2 (002) peak disappeared, which is because N doping causes the crystallinity of MoS_2 to deteriorate.[1] The presence of MoN (200) peak indicates that the Nitrogen atom successfully entered MoS_2. The SEM image and EDS mapping images of $MoS_2/Ti_3C_2T_X$ Heterostructures (Figure S4c) shows the conformal assembly of 2D $MoS_2/Ti_3C_2T_X$ heterostructures on the 3D Ni foam. Above all, Figure S4 demonstrated the successful self-assembly of $MoS_2/Ti_3C_2T_X$ heterostructures on Ni foam. Additionally, in this work all the catalysts that were mentioned are on the Ni foam if there is no exceptional explanation.

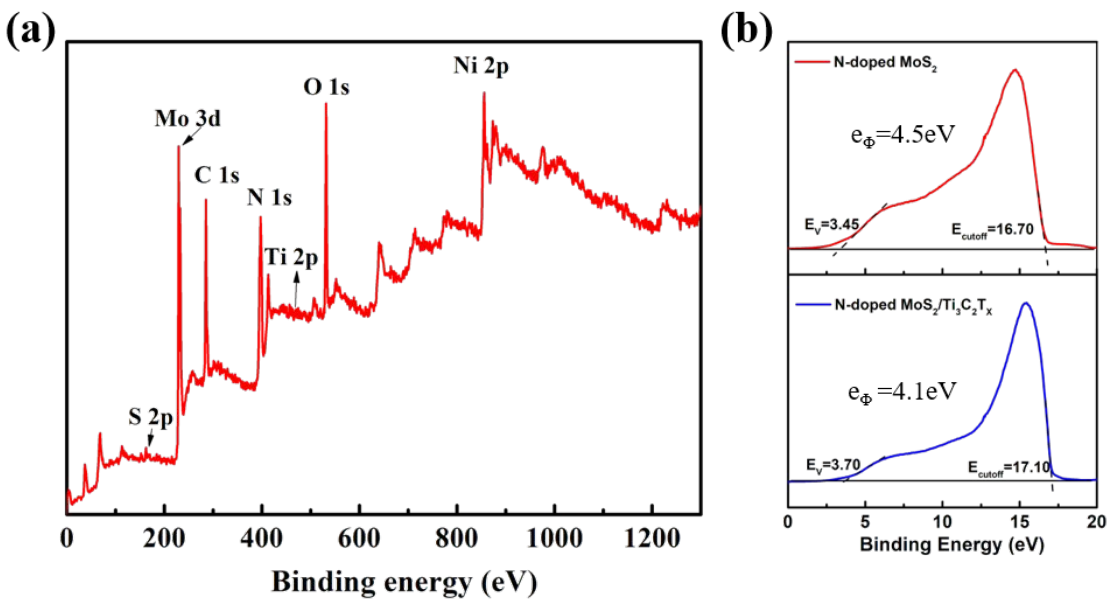

Figure S5. (a) The XPS spectrum of N-doped $MoS_2/Ti_3C_2T_X$ (b) UPS spectra of N-doped MoS_2 and N-doped $MoS_2/Ti_3C_2T_X$.

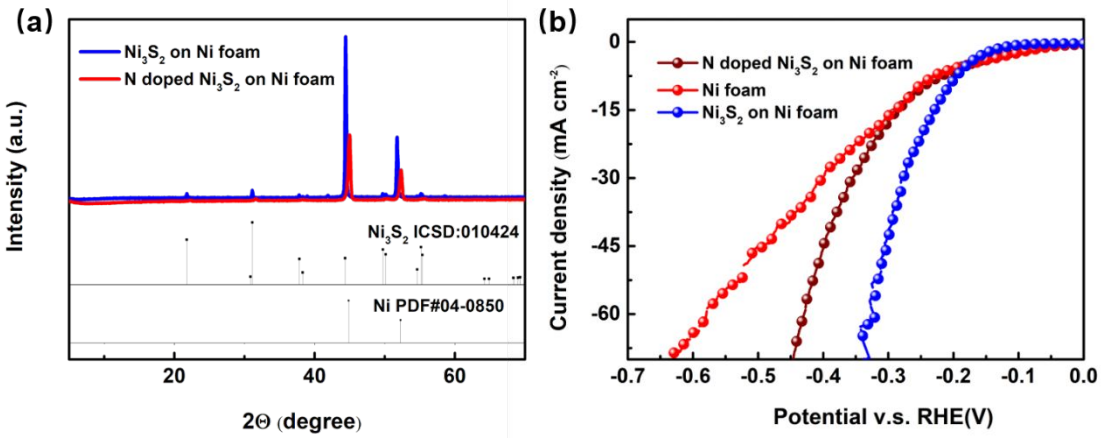

Figure S6. (a) XRD pattern. (b) LSV curves of Ni foam before and after the sulfidizing and nitriding treatment in 1.0 M KOH

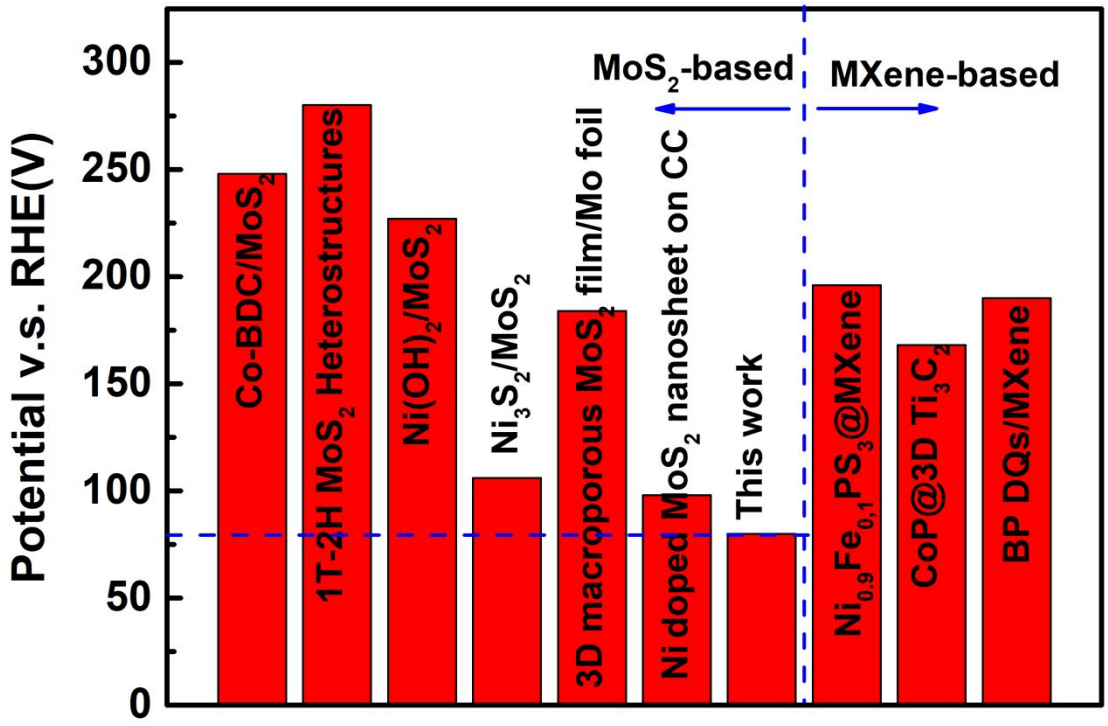

Figure S7. The comparison of the HER activity of this work with the reported MoS_2-/MXene-based HER catalysts.

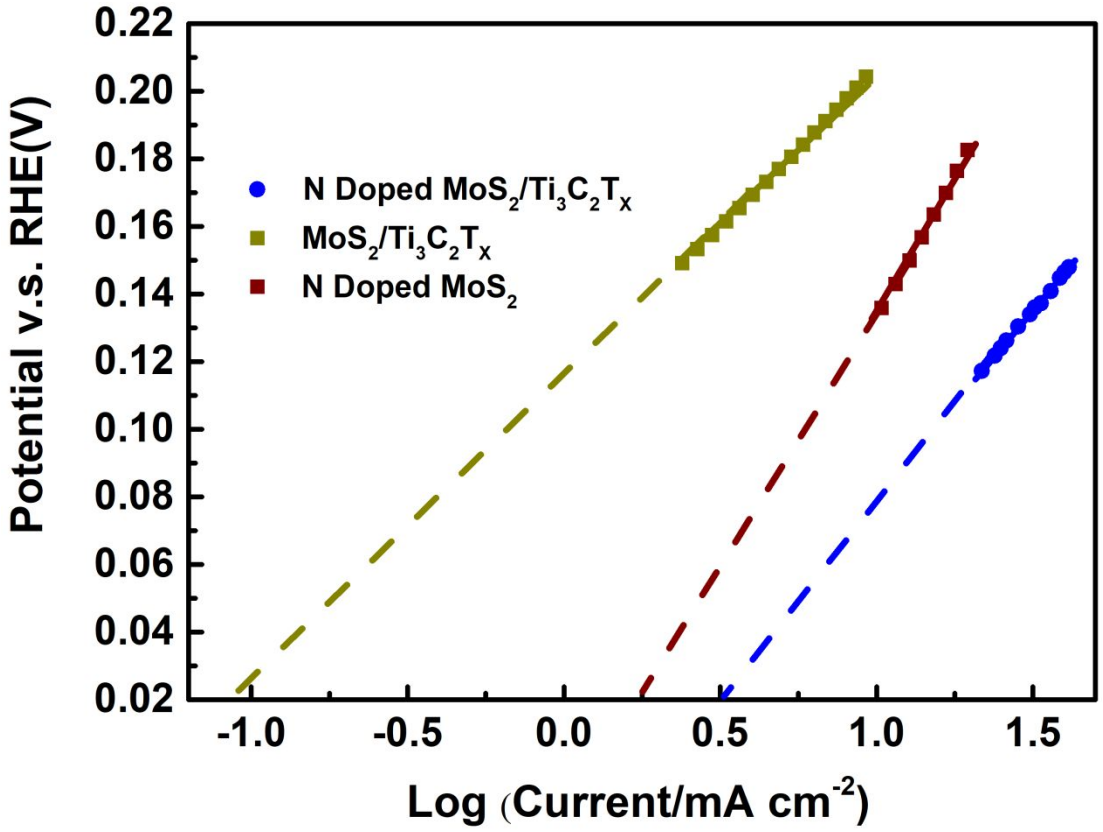

Figure S8. Tafel plot in the region of current densities of N-doped MoS_2, N-doped $MoS_2/Ti_3C_2T_X$ and MoS_2 in 1M KOH.

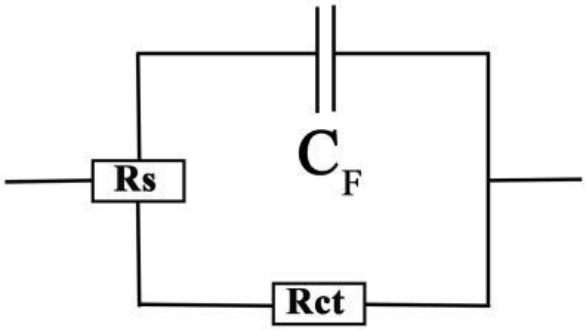

Figure S9. Equivalent circuit model fitted from the EIS data.

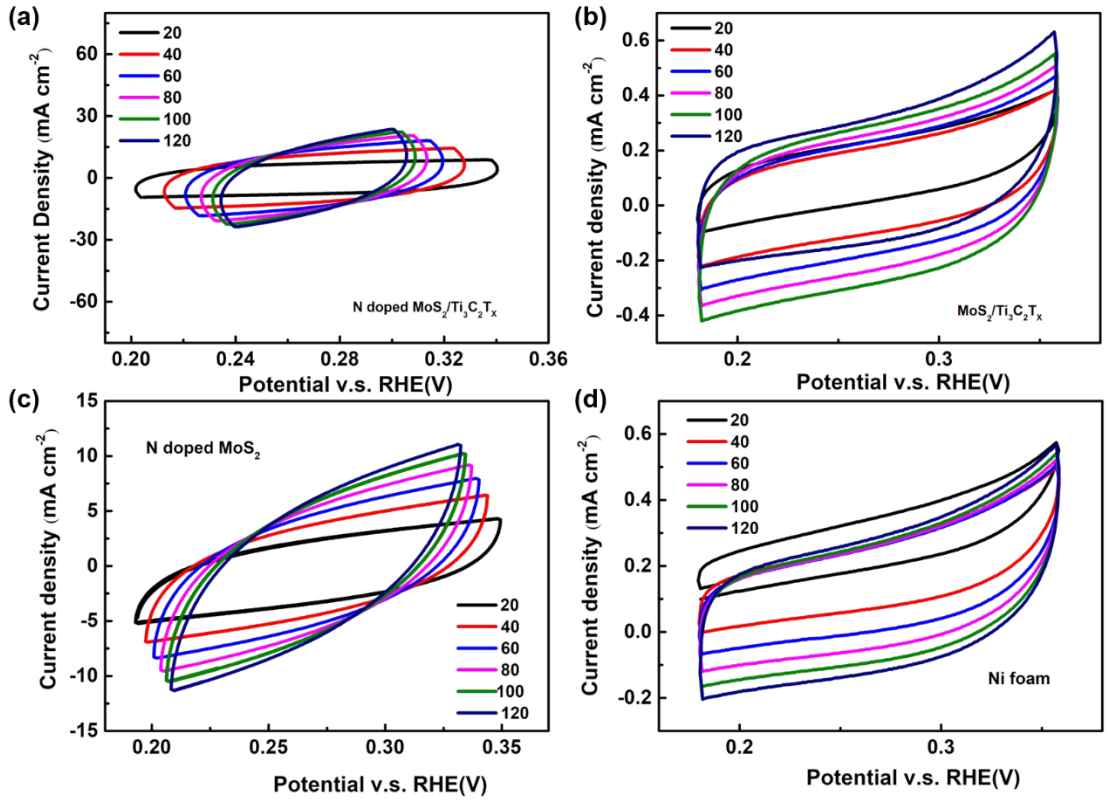

Figure S10 CV curves at different scan rate in the range from 20 mV s^{-1} to 120 mV s^{-1}, of (a) N-doped $MoS_2/Ti_3C_2T_X$, (b) $MoS_2/Ti_3C_2T_X$, (c) N-doped MoS_2 and (d) Ni foam.

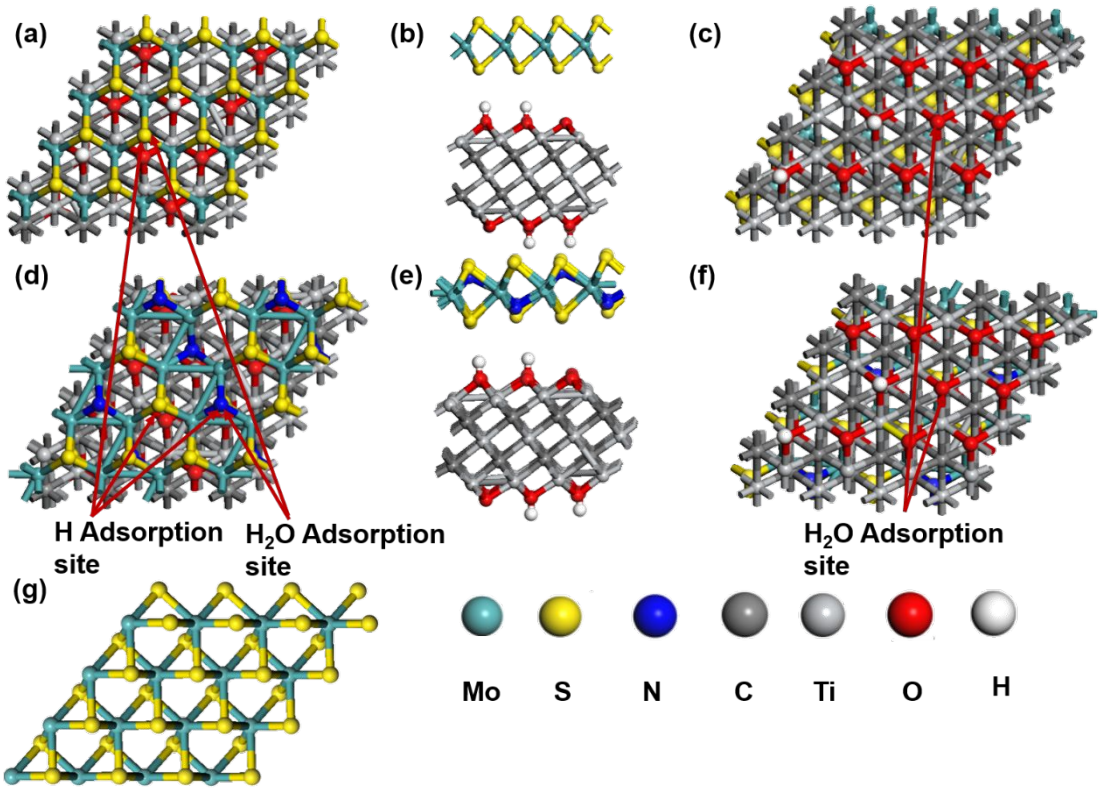

Figure S11. (a) The top, (b) side and (c) bottom view of $MoS_2/Ti_3C_2T_X$ model; (d) The top, (e) side and (f) bottom view of model of N-doped $MoS_2/Ti_3C_2T_X$. (g) The model of MoS_2.

Table S1. Comparison of HER electrocatalytic performances between N-doped $MoS_2/Ti_3C_2T_x$ in this work with reported MXene-/MoS_2-based HER catalysts in alkaline solution

Sample	Electrolyte	η_{10} (mV vs RHE)	Tafel slope (mV dec^{-1})	Ref
N doped MoS_2/ $Ti_3C_2T_X$	1M KOH	80	100	This work
PtO_aPdO_b	1M KOH	57	95	[2]
$Ni_{0.9}Fe_{0.1}PS_3$@MXene	1M KOH	196	114	[3]
CoP@3D Ti_3C_2	1M KOH	168	58	[4]
BP QDs/MXene	1M KOH	190	83	[5]
Co-BDC/MoS_2	1M KOH	248		[6]
1T-2H MoS_2 Heterostructures	1.0M KOH	280		[7]
$Ni(OH)_2/MoS_2$	1.0M KOH	227		[8]
MoS_2/Ni_3S_2	1.0M KOH	110		[9]
D macroporous MoS_2 film/Mo foil	1.0M KOH	184		[10]
Ni doped MoS_2 nanosheets on CC	1.0M KOH	98		[11]

REFERENCES

[1] Kuang, M.; Zhang, J.; Liu, D.; Tan, H.; Dinh, K.N.; Yang, L.; Ren, H.; Huang.; Fang, W.; Yao, J.; Hao, X.; Xu, J.; Liu, C.; Song, L.; Liu, B.; Yan, Q. Amorphous/Crystalline Heterostructured Cobalt‐Vanadium‐Iron (Oxy)hydroxides for Highly Efficient Oxygen Evolution Reaction. *Adv. Energy Mater*. **2020**, 10(43), 2002215.

[2] Cui, B.; Hu, B.; Liu, J.; Wang, M.; Song, Y.; Tian, K.; Zhang, Z.; He, L. Solution- plasma-assisted bimetallic oxide alloy nanoparticles of Pt and Pd embedded within two- dimensional $Ti_3C_2T_x$ nanosheets as highly active electrocatalysts for overall water splitting. *ACS Appl. Mater. Inter*. **2018**, 10, 23858-23873.

[3] Du, C. F.; Dinh, K. N.; Liang, Q. H.; Zheng, Y.; Luo, Y. B.; Zhang, J. L.; Yan, Q.Y. Self-assemble and in situ formation of $Ni_{1-x}Fe_xPS_3$ nanomosaic-decorated MXene hybrids for overall water splitting. *Adv. Energy Mater*. **2018**, 8, 1801127.

[4] Xiu, L.; Wang, Z.; Yu, M.; Wu, X.; Qiu, J. Aggregation-resistant 3D MXene-based architecture as efficient bifunctional electrocatalyst for overall water splitting. *ACS Nano*. **2018**, 12, 8017-8028.

[5] Zhu, X. D.; Xie, Y.; Liu, Y. T. Exploring the synergy of 2D MXene-supported black phosphorus quantum dots in hydrogen and oxygen evolution reactions. *J. Mater. Chem. A*. **2018**, 6, 21255-21260

[6] Zhu, D.; Liu, J.; Zhao, Y.; Zheng Y.; Qiao, S. Engineering 2D Metal-Organic Frameworks/MoS_2 Interface for Enhanced Alkaline Hydrogen Evolution. *Small.* **2019**, 15,1805511.

[7] Wang, S.; Zhang, D.; Li, B.; Zhang, C.; Du, Z.; Yin, H.; Bi, X.; Yang, S. Ultrastable In-Plane 1T-2H MoS_2 Heterostructures for Enhanced Hydrogen Evolution Reaction. *Adv. Energy Mater*. **2018**, 8, 1801345.

[8] Zhao, G.; Lin, Y.; Rui, K.; Zhou, Q.; Chen, Y.; Dou, S. X.; Sun, W. Epitaxial Growth of $Ni(OH)_2$

Nanoclusters on MoS_2 Nanosheets for Enhanced Alkaline Hydrogen Evolution Reaction. *Nanoscale* **2018**, 10, 19074–19081.

[9] Zhang, J.; Wang, T.; Pohl, D.; Rellinghaus, B.; Dong, R.; Liu, S.; Zhuang, X.; Feng, X. Interface Engineering of MoS_2/Ni_3S_2 heterostructures for highly enhanced electrochemical overall-water-splitting activity. *Angew. Chem. Int. Ed*. **2016**, 55, 6702-6707.

[10] Pu, Z. H.; Liu, Q.; M.Asiri, A.; Luo, Y.; Sun, X.; He, Y. 3D macroporous MoS_2 thin film: in situ hydrothermal preparation and application as a highly active hydrogen evolution electrocatalyst at all pH values. *Electrochim.* **2015**, *Acta* 168, 133-138.

[11] Zhang, J.; Wang, T.; Liu, P.; Liu, S.; Dong, R.; Zhuang, X.; Chen, M.; Feng, X. Engineering water dissociation sites in MoS_2 nanosheets for accelerated electrocatalytic hydrogen production. *Energy Environ. Sci*. **2016**, 9, 2789-2793.